




Synthesis and Characterization of Calcium Manganese Oxide Powders by Co-precipitation Technique

Megha Pant^a, R. P. Tandon^a, and Ajit K. Mahapatro^{a,b} 

^aDepartment of Physics and Astrophysics, University of Delhi, Delhi, India; ^bDepartment of Physics & Astronomy, University of the Western Cape, Bellville, Cape Town, South Africa

ABSTRACT

This work presents step by step procedure for synthesis of calcium manganese oxide (CaMnO₃) prepared by co-precipitation method starting with stoichiometric amounts of calcium nitrate tetrahydrate and manganese nitrate tetrahydrate as precursors. The resulting powders of CaMnO₃ are characterized for their crystallographic and spectroscopic properties. The X-ray diffraction patterns reveal formation of CaMnO₃ consistent with the corresponding JCPDS. The Fourier transform infrared spectra represents the presence of Ca-O and Mn-O bond in the synthesized powders. The optical band gap of the samples is evaluated as 4.06–4.14 eV by studying the UV-Visible spectrum. The field emission scanning electron microscope images reveal irregular feature sizes with some nearly spherical particles in the synthesized samples. The currently prepared highly pure CaMnO₃ attained can be consolidated into hot-pressed ceramics for measuring their electronic and thermoelectric properties to study their thermoelectric performance.

KEYWORDS

Calcium manganese oxide (CaMnO₃); thermoelectric; co-precipitation

1. Introduction

The global energy crisis has escalated the research on developing ways to produce energy from the waste energies by adopting environment friendly methods. Thermoelectricity is potential sources of renewable energy that can directly convert the waste heat into electricity that otherwise get wasted into the environment and cause global warming. The efficiency of thermoelectric (TE) devices depends mainly on the material utilized to convert heat into electricity. Various classes of materials including chalcogenides [1,2], skutterudites [3,4], half-Heuslers [5,6], clathrates [7,8], and oxides [9,10] have been discovered and explored to be utilized as efficient TE materials.

The efficiency of a thermoelectric (TE) material is determined by the thermoelectric figure of merit, ZT that depends on Seebeck coefficient (S), electrical conductivity (σ), thermal conductivity (k) and temperature (T). Conventional TE materials that are being used commercially have maximum achievable ZT of ~ 2.2 and efficiency of less than 20% [4,11]. The conventional TE materials are expensive, toxic and less stable at high temperatures as compared to oxides TE materials that drives research in replacing the conventional thermoelectric materials by oxide based commercial TE materials [12].

Perovskite manganites with general formula $AMnO_3$ (where $A = Ca, La, Ba, Sr, Pb, Nd, Pr$) is a class of oxides thermoelectrics that exhibit unique electrical and magnetic properties and have been extensively utilized in various application areas like gas sensing, multiferroics, anode material for lithium ion batteries, colossal magnetoresistance, fuel cells, thermoelectric generators [13–15]. Calcium manganese oxide ($CaMnO_3$) is an n-type manganite that exhibits high S ($\sim -550 \mu V/K$) and low k ($\sim 3 W/m\cdot K$) classifying it to be a potential TE material. Perovskite structures have two doping sites making them suitable for tuning the properties for utilization in different applications. However, the room temperature electrical resistivity of these oxides is too high restricting the ZT values to as low as 0.06. Recent researches focus on improving the thermoelectric performance of $CaMnO_3$ by reducing the electrical resistivity through nanostructuring or via electron doping [12,16,17].

In this work, $CaMnO_3$ is synthesized by co-precipitation method using calcium nitrate tetrahydrate and manganese nitrate tetrahydrate as precursors. The as-prepared powders have been annealed at $600^\circ C$, $800^\circ C$, and $1000^\circ C$ for 4 h. Crystallographic, spectroscopic, and morphological details have been studied by X-Ray diffraction (XRD) technique, ultraviolet-visible (UV-Vis) spectroscopy, Fourier transform infrared (FTIR) spectroscopy, field emission electron microscopy (FESEM).

2. Experimental Details

2.1. Synthesis

All the chemicals were procured from Alfa Aesar, USA and were of 99.9% purity. The chemicals used to synthesize $CaMnO_3$ were calcium nitrate ($Ca(NO_3)_2 \cdot 4H_2O$), manganese nitrate ($Mn(NO_3)_2 \cdot 4H_2O$), ethanol (C_2H_5OH), and sodium hydroxide (NaOH). In another beaker, 2 g of $Ca(NO_3)_2 \cdot 4H_2O$ and 2.125 g of $Mn(NO_3)_2 \cdot 4H_2O$ were separately taken in 80 ml of ethanol and stirred at $50^\circ C$. The solutions were then mixed to obtain a homogeneous mixture. 1.12 g of NaOH was added to 40 ml of distilled water and this solution was then added dropwise into the mixture kept under constant stirring at $70^\circ C$. The mixture was then kept aside for complete precipitation. The precipitate obtained was washed several times with ethanol and heated at $100^\circ C$ to remove excess solvent. The dried-precipitate (named as A) was then annealed at $600^\circ C$, $800^\circ C$, and $1000^\circ C$, which were nomenclatured as A600, A800, and A1000, respectively.

2.2. Characterization Techniques

The as-synthesized powders were characterized by XRD, FESEM, FTIR spectroscopy, and UV-Vis spectroscopy. The phase composition of the powders was studied by XRD (Rigaku, Ultima IV X-ray diffractometer, Japan) using Cu K- α radiation with excitation wavelength of 1.54 \AA with active angular range of $2\theta = 20^\circ - 85^\circ$ scanned at a rate of $2^\circ/\text{min}$. The morphology of the samples were analyzed using FESEM (Zeiss, Germany) operated at 15 kV. The FTIR spectra was studied using Nicolet IS50-Thermo scientific instrument in the range $400-4000 \text{ cm}^{-1}$. The optical band gaps were estimated from the UV-Vis spectra recorded in the wavelength range 200–700 nm using Perkin Elmer UV-Visible spectrometer.

3. Results and Discussion

3.1. Crystallographic Study by XRD

The XRD patterns of all the synthesized powders are illustrated in Figure 1. The XRD patterns of the as-prepared sample (A) matches with JCPDS reference code (#00-076-1133) which indicates the formation of $\text{Ca}_2\text{Mn}_2\text{O}_5$ in the as-prepared sample. The diffraction peaks for samples A600, A800 and A1000 are indexed with the standard hkl values in accordance with the JCPDS card no. (#00-89-0666) assigned for CaMnO_3 . The XRD show good crystallinity, phase purity. The absence of any additional peak in the XRD pattern of the samples annealed at 600 °C, 800 °C, and 1000 °C indicate the formation of highly pure and single phase of CaMnO_3 . This infers better crystallinity in the annealed samples compared to the as-prepared sample. The average crystallite size was estimated from the most intense peaks in XRD using the modified Scherer's method, estimating the values of the crystallite size as 46, 68, and 73 nm for A600, A800, and A1000, respectively, indicating increase in the crystallite size on increasing the annealing temperature.

3.2. FTIR Spectroscopy

Figure 2 shows the FTIR spectra of the annealed samples. The band at around 411 cm^{-1} correspond to the bending vibration of the Mn-O-Mn bond and the weak band at around 444 cm^{-1} is attributed to the Mn-O stretching vibration. The broad band at

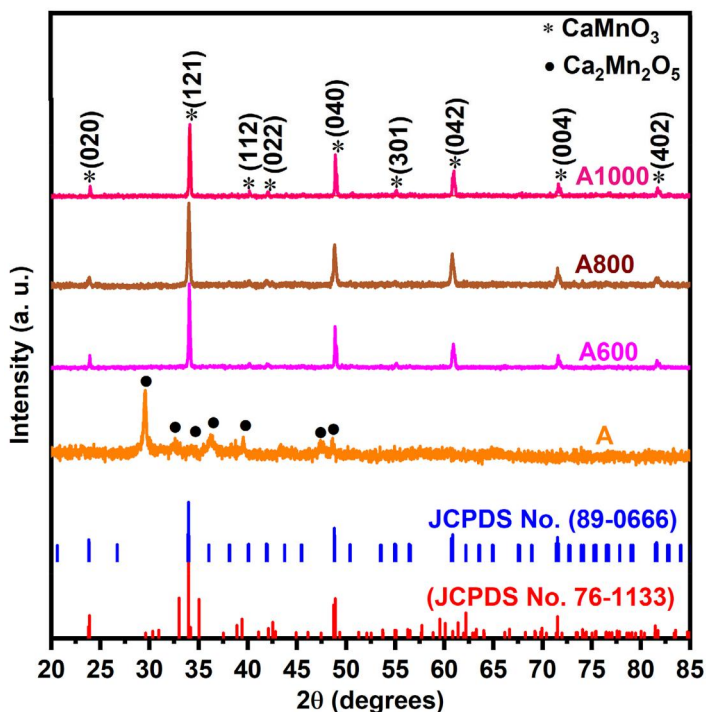


Figure 1. XRD patterns of all the samples. The two patterns at the bottom represent the JCPDS data for $\text{Ca}_2\text{Mn}_2\text{O}_5$ (#76 – 1133) and CaMnO_3 (#89-0666).

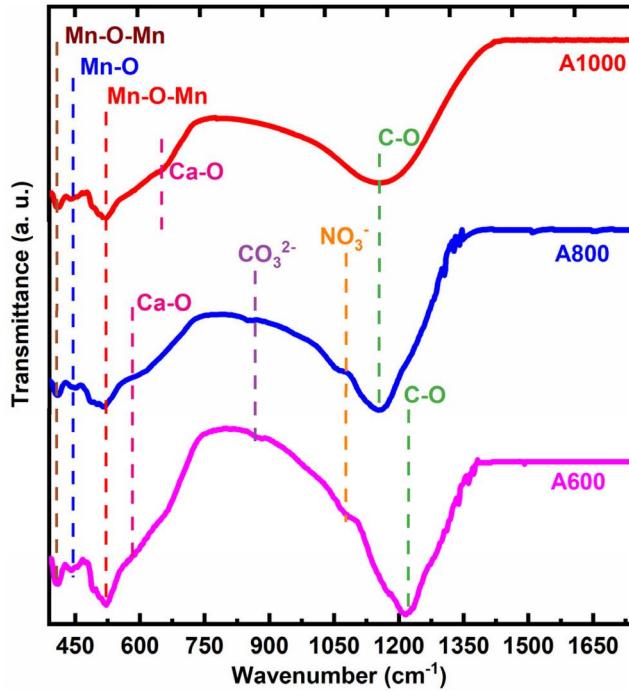


Figure 2. FTIR spectra of the samples annealed at 600 °C, 800 °C, and 1000 °C denoted as A600, A800, and A1000, respectively.

around 523 cm^{-1} is ascribed to the tilting of Mn-O-Mn bond of the MnO_6 octahedra [18–20]. The weak band observed at around 586 cm^{-1} corresponds to the vibration of the Ca-O bond. The shift in the band position of Ca-O bond toward the higher wavenumber side was observed on increasing the annealing temperature. The bands below 600 cm^{-1} observed in the annealed samples attribute to the formation of the perovskite structure [13]. The samples A600 and A800 show the presence of NO_3^- group that could be due to the nitrate precursors utilized for synthesizing CaMnO_3 [21]. The broad band observed around wavenumber of 1220 cm^{-1} in A600 and A1000 and 1184 cm^{-1} in A800 corresponds to the C-O stretching vibration and a small hump positioned at 875 cm^{-1} is due to the carbonate peak originating from the possible adsorption of atmospheric CO_2 [22,23]. No vibrational band was observed beyond 1350 cm^{-1} for any of the samples. The absence of any vibrational band characteristic of the precursor in the sample A1000 indicates 1000 °C is the optimum temperature for synthesizing stoichiometric CaMnO_3 using the synthesis recipe adopted in this work.

3.3. Morphology by FESEM

The morphology of all the samples is shown in Figure 3(a–c) and the distribution of particle size is shown in Figure 3(d–f). All the three FESEM images show irregular feature sizes. An increase in particle size was observed with the increase in the annealing temperature. The average particle size was found to be around 320 nm, 1.08 μm , and 1.14 μm for A600, A800, and A1000, respectively.

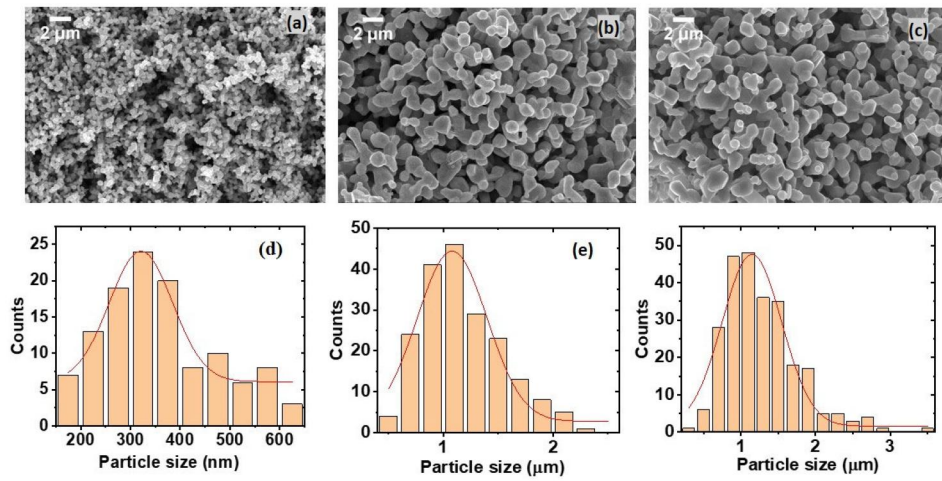


Figure 3. FESEM images of (a) A600, (b) A800, (c) A1000 and particle size distribution of (d) A600, (e) A800, and (f) A1000.

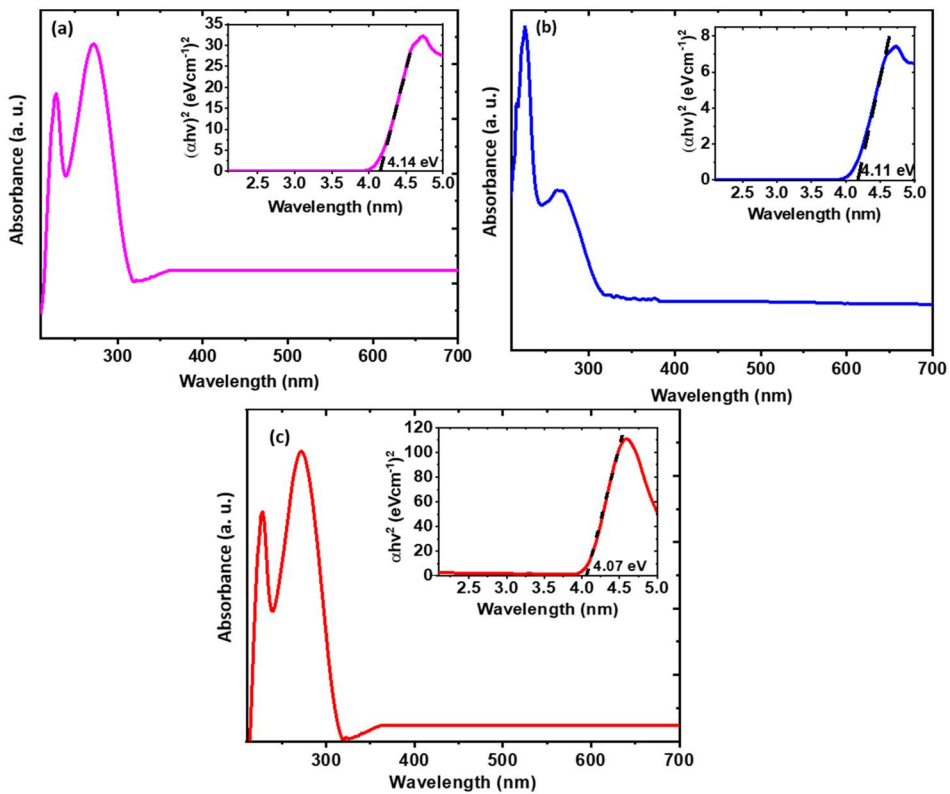


Figure 4. UV-Visible spectra of (a) A600, (b) A800, and (c) A1000. The insets of (a), (b), and (c) show the Tauc plot for the estimation of band gap.

3.4. UV-Visible Spectroscopy

Figure 4 demonstrates the UV-Vis spectra of the annealed powders of CaMnO_3 . Two peaks at around 230 nm and 270 nm were observed in the absorbance spectra for the powders indicating the presence of two electronic transitions from valence to the conduction band. The inset of Figure 4 shows the Tauc plot of $(\alpha h\nu)^2$ versus $h\nu$ and the extrapolation of the linear portion to the energy estimates the value of the band gap according to the Mott Davis equation:

$$\alpha h\nu = A(h\nu - E_g)^n$$

where α is the absorption coefficient, $h\nu$ is the photon energy and E_g is the band gap. The value of $n = 2$ fits the above equation which indicates the synthesized CaMnO_3 is a direct band gap material which is in corroboration with the earlier reported results [24,25]. The value of E_g obtained after extrapolation was found to be 4.14, 4.11, and 4.06 eV for A600, A800, and A1000, respectively. A decrease in the band gap value is observed on increasing the annealing temperature from 600 °C to 800 °C. The decrease in the optical band gap value can be attributed to the increase in the particle size which is consistent with the particle size distribution obtained from the FESEM images.

4. Conclusion

Single phase CaMnO_3 was synthesized using co-precipitation method starting with $\text{Ca}(\text{NO}_3)_2 \cdot 4\text{H}_2\text{O}$, and $(\text{Mn}(\text{NO}_3)_2 \cdot 4\text{H}_2\text{O})$, as precursors. The XRD pattern indicates the formation of oxygen deficient calcium manganese oxide ($\text{Ca}_2\text{Mn}_2\text{O}_5$) in the as-prepared powder. The XRD pattern after annealing of as-synthesized powder results better crystallinity with the formation of stoichiometric of CaMnO_3 . FTIR spectra recorded for the annealed samples shows vibrational bands of Ca-O and Mn-O, suggesting the formation of perovskite structured calcium manganese oxide. FESEM images depict irregular feature sizes and nearly spherical particles of sizes 320 nm, 1.08 μm , and 1.14 μm for A600, A800, and A1000, respectively. The energy band gap of the CaMnO_3 powders estimated from the UV-Vis spectra ranges from 4 to 4.15 eV for annealing at 600–1000 °C. The reduced bandgap energy is attributed to the increase in the particle size with increase in the annealing temperature. The CaMnO_3 powders synthesized using the co-precipitation method can be utilized in the thermoelectric applications by pelletizing the powder into dense ceramics and measuring the electrical resistivity, Seebeck coefficient, and thermal conductivity of the pellets.

Acknowledgments

MP acknowledges CSIR, Delhi for providing fellowship to pursue research for PhD Program. The authors express their gratitude to University Science Instrumentation Centre (USIC) and Central Experimental Facility (CEF) at University of Delhi for providing the instrumentation facility for pursuing the characterization techniques. The authors acknowledge the financial assistance provided by IoE (ref. No./IoE/2022-23/FRP/and ref. No./IoE/2023-24/12/FRP) through FRP scheme.

Disclosure Statement

No potential conflict of interest was reported by the author(s).

ORCID

Ajit K. Mahapatro  <http://orcid.org/0000-0002-3860-2862>

References

1. Y. Shi, C. Sturm, and H. Kleinke, Chalcogenides as thermoelectric materials, *J. Solid State Chem.* **270**, 273 (2019). DOI: [10.1016/j.jssc.2018.10.049](https://doi.org/10.1016/j.jssc.2018.10.049).
2. S. Roychowdhury *et al.*, Germanium chalcogenide thermoelectrics: electronic structure modulation and low lattice thermal conductivity, *Chem. Mater.* **30** (17), 5799 (2018). DOI: [10.1021/acs.chemmater.8b02676](https://doi.org/10.1021/acs.chemmater.8b02676).
3. S. Katsuyama *et al.*, Thermoelectric properties of the skutterudite $\text{Co}_{1-x}\text{Fe}_x\text{Sb}_3$ system, *J. Appl. Phys.* **84** (12), 6708 (1998). DOI: [10.1063/1.369048](https://doi.org/10.1063/1.369048).
4. M. R. Bravo *et al.*, Skutterudites as thermoelectric materials: revisited, *RSC Adv.* **5**, 41653 (2015).
5. W. Li *et al.*, Conformal high-power-density half-Heusler thermoelectric modules: a pathway toward practical power generators, *ACS Appl. Mater. Interfaces.* **13** (45), 53935 (2021). DOI: [10.1021/acsami.1c16117](https://doi.org/10.1021/acsami.1c16117).
6. R. J. Quinn, and J. W. G. Bos, Advances in half-Heusler alloys for thermoelectric power generation, *Mater. Adv.* **2** (19), 6246 (2021). DOI: [10.1039/D1MA00707F](https://doi.org/10.1039/D1MA00707F).
7. B. Liu *et al.*, Thermoelectric properties of In-substituted Ge-based clathrates prepared by HPHT, *J. Materiomics* **4** (1), 68 (2018). DOI: [10.1016/j.jmat.2017.11.001](https://doi.org/10.1016/j.jmat.2017.11.001).
8. J. A. Dolyniuk *et al.*, Clathrate thermoelectrics, *Mater. Sci. Eng. R.* **108**, 1 (2016).
9. Y. Yin, B. Tudu, and A. Tiwari, Recent advances in oxide thermoelectric materials and modules, *Vacuum* **146**, 356 (2017). DOI: [10.1016/j.vacuum.2017.04.015](https://doi.org/10.1016/j.vacuum.2017.04.015).
10. J. He, Y. Liu, and R. Funahashi, Oxide thermoelectrics: The challenges, progress, and outlook, *J. Mater. Res.* **26** (15), 1762 (2011). DOI: [10.1557/jmr.2011.108](https://doi.org/10.1557/jmr.2011.108).
11. J. He, M. G. Kanatzidis, and V. P. Dravid, High performance bulk thermoelectrics via a panoscopic approach, *Mater. Today* **16** (5), 166 (2013). DOI: [10.1016/j.mattod.2013.05.004](https://doi.org/10.1016/j.mattod.2013.05.004).
12. T. Liu *et al.*, Achieving enhanced thermoelectric performance of $\text{Ca}_{1-x-y}\text{La}_x\text{Sr}_y\text{MnO}_3$ via synergistic carrier concentration optimization and chemical bond engineering, *Chem. Engng. J.* **408**, 127364 (2021). DOI: [10.1016/j.cej.2020.127364](https://doi.org/10.1016/j.cej.2020.127364).
13. L. Chang *et al.*, Perovskite-type CaMnO_3 anode material for highly efficient and stable lithium ion storage, *J. Colloid Interface Sci.* **584**, 698 (2021). DOI: [10.1016/j.jcis.2020.04.014](https://doi.org/10.1016/j.jcis.2020.04.014).
14. M. A. A. Bally *et al.*, Magnetic properties of $\text{La}_{0.55}\text{Ca}_x\text{Sr}_{0.45}\text{MnO}_3$ perovskite manganite, *Res. Phys.* **21**, 103800 (2021). DOI: [10.1016/j.rinp.2020.103800](https://doi.org/10.1016/j.rinp.2020.103800).
15. P. M. Bulemo, and I. D. Kim, Recent advances in ABO_3 perovskites: their gas-sensing performance as resistive-type gas sensors, *J. Korean Ceram. Soc.* **57** (1), 24 (2020). DOI: [10.1007/s43207-019-00003-1](https://doi.org/10.1007/s43207-019-00003-1).
16. C. Li, Q. Chen, and Y. Yan, Effects of Pr and Yb dual doping on the thermoelectric properties of CaMnO_3 , *Materials* **11** (10), 1807 (2018). DOI: [10.3390/ma11101807](https://doi.org/10.3390/ma11101807).
17. E. Oz *et al.*, Fabrication of Ca-Mn-Nb-O compounds and their structural, electrical, magnetic and thermoelectric properties, *Mater. Res. Express* **5** (3), 036304 (2018). DOI: [10.1088/2053-1591/aab3af](https://doi.org/10.1088/2053-1591/aab3af).
18. A. Mishra, and S. Bhattacharjee, Effect of A- or B-site doping of perovskite calcium manganite on structure, resistivity, and thermoelectric properties, *J. Am. Ceram. Soc.* **100** (10), 4945 (2017). DOI: [10.1111/jace.15015](https://doi.org/10.1111/jace.15015).
19. J. Macan *et al.*, Soft chemistry synthesis of CaMnO_3 powders and films, *Ceram. Int.* **46** (11), 18200 (2020). DOI: [10.1016/j.ceramint.2020.04.142](https://doi.org/10.1016/j.ceramint.2020.04.142).

20. K. Nandan, and A. R. Kumar, Structural and electrical properties of $\text{Ca}_{0.9}\text{Dy}_{0.1}\text{MnO}_3$ prepared by sol-gel technique, *J. Mater. Res. Technol.* **8** (3), 2996 (2019). DOI: [10.1016/j.jmrt.2017.05.020](https://doi.org/10.1016/j.jmrt.2017.05.020).
21. A. Žužić, A. Ressler, and J. Macan, Evaluation of carbonate precursors in manganite coprecipitation synthesis by Fourier transform infrared (FTIR) spectroscopy, *Solid State Commun.* **341**, 114594 (2022). DOI: [10.1016/j.ssc.2021.114594](https://doi.org/10.1016/j.ssc.2021.114594).
22. M. Kemary, N. Nagy, and I. El-Mehasseb, Nickel oxide nanoparticles: synthesis and spectral studies of interactions with glucose, *Mater. Sci. Semicond. Process.* **16** (6), 1747 (2013). DOI: [10.1016/j.mssp.2013.05.018](https://doi.org/10.1016/j.mssp.2013.05.018).
23. M. Shahnawaz, S. Khan, and S. Mukherjee, Development of perovskite barium titanate by an agate mortar mill activated solid-state process, *Interceram - Int. Ceram Rev.* **67** (4), 44 (2018). DOI: [10.1007/s42411-018-0020-5](https://doi.org/10.1007/s42411-018-0020-5).
24. P. Garg *et al.*, Solution-processed CaMnO_3 - δ -based all oxide solar cells with high open-circuit voltage, *Phys. Rev. Mater.* **6** (8), 085402 (2022). DOI: [10.1103/PhysRevMaterials.6.085402](https://doi.org/10.1103/PhysRevMaterials.6.085402).
25. S. K. Parida, Studies on structural, dielectric and optical properties of Cu/W double substituted calcium manganite for solar cells and thermistor applications, *Phase Trans.* **94** (12), 1033 (2021). DOI: [10.1080/01411594.2021.1995606](https://doi.org/10.1080/01411594.2021.1995606).